The development of the geophysical wind vector algorithms and their evaluation using Seasat $\sigma°$ data is presently being completed. A detailed description of these geophysical algorithms and results obtained by processing SASS data with them will be presented in a future journal article. Preliminary results of early analyses of data processed with development versions of these algorithms have been published in [10] and in the GOASEX Workshop reports [11], and [12].

REFERENCES

[1] J.W. Johnson, L.A. Williams, Jr., E.M. Bracalente, F.B. Beck, and W.L. Grantham, "Seasat-A satellite scatterometer instrument evaluation," this issue, pp. 138–144.

[2] J.W. Brown, G.C. Cleven, J.C. Klose, D.B. Lame, and C.A. Yamarone, "Seasat low-rate data system," *Science*, vol. 204, pp. 1407–1408, June 29, 1979.

[3] W.L. Grantham, E.M. Bracalente, W.L. Jones, J.H. Schrader, L.C. Schroeder, and J.C. Mitchell, "An operational satellite Scatterometer for wind vector measurements over oceans," NASA TMX 72672, Mar. 1975.

[4] R.E. Fischer, "Standard deviation of scatterometer measurements from space," *IEEE Trans. Geosc. Electron.*, vol. GE-10, pp. 106–113, Apr. 1972.

[5] E.G. Njoku, E.J. Christensen, and R.E. Cofield, "The Seasat scanning multichannel microwave radiometer (SMMR): Antenna pattern corrections—development and implementation," this issue, pp. 125–137.

[6] A. Sobti, R.K. Moore, and S.T. Ulaby, "Backscatter response at 13.9 GHz for major terraine types as seen from orbit," Univ. of Kansas Res. Center, Inc., Lawrence, KA, Tech. Report 243-4, NASA Contract NAS9-13331, Aug. 1975.

[7] A. Sobti and E.C. Davidson, "Microwave scattering measurements over Brazil at 13.9 GHz," Univ. of Kansas Res. Center, Inc., Lawrence, Kansas, Tech. Report 243-11, NASA Contract NAS9-13331, Sept. 1975.

[8] W.L. Jones, L.C. Schroeder, and J.L. Mitchell, "Aircraft measurements of the microwave scattering signature of the ocean," *IEEE Trans. Antennas and Propagat./IEEE J. Oceanic Eng.*, Special Issue of *Radio Oceanography*, Jan. 1977.

[9] F.J. Wentz, "Estimate of the sea-surface's two scale backscatter parameters," NASA Contractor Rep. 145255, Mar. 1978.

[10] W. Linwood Jones *et al.*, "Seasat scatterometer: Results of the Gulf of Alaska Workshop," *Science*, vol. 204, pp. 1413–1415, June 29, 1979.

[11] Seasat Gulf of Alaska Workshop Rep. 622-101, vol. 1, sect. I, II, III, IV, and VII, Jet Propulsion Lab., Apr. 1979.

[12] Preliminary Seasat Gulf of Alaska Workshop II Rep. 622-107, sects. I, II, III, and VIII, Jet Propulsion Lab., Oct. 1979.

The Seasat-A Synthetic Aperture Radar System

ROLANDO L. JORDAN

Abstract—The objective of the Seasat-A synthetic aperture radar (SAR) system was to detect ocean waves from orbital altitudes. An SAR system operating at 1275 MHz (23-cm wavelength) was designed and built to meet this objective. The choice of wavelength was the result of imagery obtained by aircraft during 1972 to 1974 and ease of implementation. The Seasat-A SAR system was turned on in orbit on July 4, 1978, and gathered imagery until the spacecraft bus failed in orbit in October 1978.

I. INTRODUCTION

THE SEASAT-A synthetic aperture imaging radar system (SAR) was the first imaging radar system used as a scientific instrument from earth orbit. This system generated continuous radar imagery with a 100-km swath at a resolution of 25 m from an 800-km altitude orbit. The imagery is a pictorial representation of the radar backscatter of the Earth's surface in a map-like representation.

The development of the Seasat-A SAR system is significant because it is the precursor of a series of SAR systems which will be flown in other spacecraft as remote sensors such as the Venus orbiting imaging radar (VOIR), the shuttle imaging radar to be flown on an Orbital Flight Mission-2 (OFT-2),
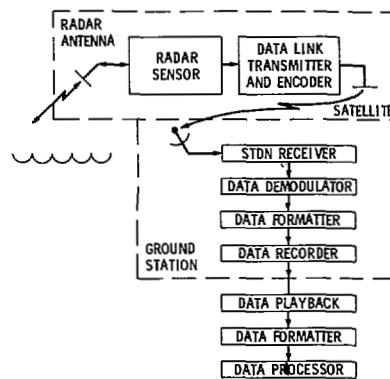
Fig. 1. Seasat SAR system functional diagram.

and others. Lessons learned during its development and final performance assessment will have a large impact on the development of future orbital SAR systems.

The Seasat-A SAR system, as shown in Fig. 1, consists of a planar array antenna, a transmitter/receiver sensor, an analog data link, data formatter, high density digital recorder, and optical processing subsystem. The overall system characteristics are tabulated in Table I. This system represents a highly complex instrument which could generate continuous imagery with a 100-km swath for a distance exceeding 4000

TABLE I

| SEASAT-A SAR SYSTEM CHARACTERISTICS	
Satellite altitude	800 km
Wavelength	0.235 m
Theoretical Resolution	25 x 25 meters on the surface
Contrast ratio	9 dB
Swath width	100 km
RF bandwidth	19 MHz
Transmit pulse length	33.4 µsec
Pulse repetition rate	1463 to 1640 pps
Transmit time bandwidth product	634
Radar transmitter peak power	1000 w
Telemetry transmitter power	5 w
Telemetry frequency	2265 MHz
Radar transmitter average power	55 w
Sensitivity time control range	9 dB
Data recorder bit rate	110 Mbits/sec (5 bits per word)
Data recording pass duration	10 min
Radar DC power	500 w
Radar antenna dimensions	10.7 by 2.16 m
Radar antenna gain	35 dB
Telemetry antenna	Quadrafilar Helix
Telemetry transmit antenna gain	5 dB
Telemetry ground station antenna	9 meter parabolic antenna
Data processing	Optical, digital for selected areas
Processing format	4 - 25 km x 4000 km swaths optical 100 Km x 100 Km digital
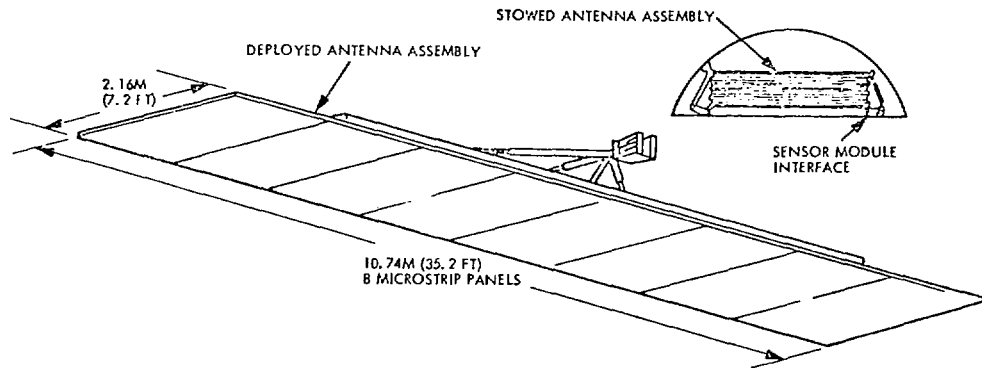
Fig. 2.   SAR antenna subsystem.

km when in view of a ground station equipped to receive SAR data. The emphasis of this paper is on the system aspects of the Seasat-A SAR system with a description of some of the engineering results obtained during its mission.

II. HARDWARE DESCRIPTION

A. Antenna

The Seasat-A SAR antenna system consists of a 10.74 m by 2.16 m phased array system deployed after orbit insertion. This deployed antenna is configured to fly with the long dimension along the spacecraft velocity vector and bore-sighted at an angle of 20.5° from the nadir direction in elevation (cone) and 90° from the nominal spacecraft velocity vector (clock). The antenna dimensions (10.74 X 2.16 m) are dictated by a desire to limit range or Doppler ambiguities to acceptably low levels. At a nominal 20.5° look angle from nadir, a total beamwidth in elevation of 6.2° is required to illuminate a 100-km swath on the Earth's surface from an 800-km-high orbit. Thus the antenna cross-track dimension is 2.16 m to limit the radiation to these sets of angles. The area illuminated on the surface of the earth is from 240 to 340 km to the right of the subspacecraft point. The antenna elements in elevation are weighted in illumination to limit sidelobes in the cross-track direction. The minimum antenna

along-track length is limited by a desire to keep azimuth sampling ambiguities to an acceptable low level while the maximum along-track length is determined by the requirement to illuminate a sufficiently large patch of terrain to allow processing of the data to four looks. The radar transmitter pulses cannot be too close together to prevent overlapping the returns from near and far range. Thus the pulse repetition rate (PRF) is limited. In order to avoid sampling ambiguities of the radar data, the antenna azimuth beamwidth must be small enough so that the set of azimuth frequencies (Doppler spectrum) does not exceed the sampling rate.

However, if the azimuth beamwidth is too small, it is not possible to generate a synthetic aperture large enough to attain the desired resolution for the four independent looks. These two requirements limit the antenna length along the velocity vector to be between 10.5 and 14 m. The 10.74-m antenna length was dictated by the available volume within the satellite shroud. The level of integrated ambiguities in azimuth is estimated to be between −18 and −24 dB, depending on the PRF and processor bandwidth.

The antenna subsystem consists of eight mechanically deployed, electrically coupled, flat microstrip panels. This array, Fig. 2, is shown in both stowed and deployed configurations. The performance and design requirements

TABLE II
SAR ANTENNA PERFORMANCE

SAR ANTENNA PERFORMANCE	
Gain	35 dB at SAR Sensor Electronics
VSWR	1.5 ($\pm$ 11 MHz bandwidth)
Power	1500 W peak
Beamwidth	
Azimuth	1.73° at -4 dB
Cone Angle (Range)	6.2° $\pm$ 0.1° between +33 dB far side and +31 dB near side
Polarization	Horizontal linear of 99% purity
Frequency	1.275 GHz
Sidelobes	-12.5 dB
Phase Errors	
Quadratic	$\pm$ 20° over $\pm$ 0.5° from beam center
Higher Order	$\mp$ 2° over $\pm$ 0.5° from beam center
Beam Pointing (nominal)	90° clock angle (AZ) 20.5° cone angle (EL) 0° rotation
Beam Alignment (goal) (alignment between electrical boresight and antenna reference axes)	$\pm$ 0.2°, 3σ clock and cone (determined to $\pm$ 0.1°, 3σ) $\pm$ 0.5°, 3σ rotation (determined to $\pm$ 0.2°, 3σ)

Fig. 3. Construction of microstrip honeycomb panel.

Fig. 4. SAR antenna mechanical components and assemblies.

TABLE III
SENSOR ELECTRONICS SUBSYSTEM IMPLEMENTATION

ELECTRONICS	IMPLEMENTATION
Modes	Four: Off, Standby, Operate, Transmit
Center Frequency	1274.8 $\pm$ 0.31 MHz
Bandwidth	19.05 $\pm$ .05 MHz
Stalo Frequency	91.059 $\pm$ .0022 MHz
Stalo Stability	3 Parts/10^{10} in 5 Microseconds
Pulse Width	33.9 $\pm$ 0.8 Microseconds
Peak Power	1000 Watts Nominal
Pulse Envelope Rise Time	90 Nanoseconds
Pulse Envelope Fall Time	90 Nanoseconds
Pulse Repetition Frequencies	1464, 1540, 1580, 1647 $\pm$ .1PPS
Noise Temperature	650° Kelvin, Nominal
Receiver Gain Control Steps	8
Gain Control Step Spacing	3 $\pm$ 0.3 dB
Gain Control Range	77 to 98 dB
STC Gain Variation	9
STC Start Point Setability	12.26 Microseconds
Amplitude vs. Frequency Error	$\pm$ 0.9 dB, Including Linear Term
Phase Delay vs. Frequency Error	4.4° Receiver, 3° Transmitter, 5.3° Overall
PRF, COHOD, Transmit Event Jitter	0.7 Nanosecond, RMS
Modulation	Linear FM
Receiver 1 dB Compression Point	$\pm$ 9 $\pm$ 1 dbm
Maximum Receiver Output	$\pm$ 14 $\pm$ 1 dbm
Command Capability	Gain Mode Gain Value STC Mode STALO Heater off Transmit Calibrate Scan Calibrate Level Disable STC Position PRF Select
Input dc Voltage	28 $\pm$ 4.5. -4.0 VDC
Input dc Current Limiting	1.75 X Nominal
Output Short Circuit Current Limiting	1.5 X Nominal
Power Converter Synchronization Frequency	79.044 KHz
Standby Voltages	Separate Converter
Main Power Converter Efficiency at 28 VDC, 25° C, 100% Load	73% Nominal
Receiver Gain Flatness	$\pm$ 0.33 dB
Receiver Gain Stability (0° - 60°C)	$\mp$ 1.0 dB
Receiver Bandwidth (3 dB)	22 $\pm$ 0.2 MHz
Receiver Input Impedance	50 Ohms, Nominal
Receiver Input VSWR	1.7:1 Nominal
Receiver Output Impedance	50 Ohms
Receiver Output VSWR	1.4:1 Nominal
Receiver Phase Ripple	4.00° Dev. from quadratic
Transmitter FM Slope	0.5622 MHz/Microsecond
Transmitted Pulse Envelope Droop	5%
Transmitter Amplitude Response	$\pm$ 0.05 RMS
Transmitter Phase Response	3° RMS
Spurious Outputs (Out of Band)	-70 dB, Except for 4th Harmonic
Weight	284 lbs

placed on this subsystem are contained in Table II. The construction of the microstrip is depicted in Fig. 3 and the deployment and extension mechanization is shown in Fig. 4.

B. Radar Sensor Description

The function of the radar sensor is to provide the antenna with a series of high power coherent pulses of energy at L band, and amplify the weak return echoes which are re-received by the antenna. The radar sensor consists of four subassemblies: transmitter, receiver, logic and control, and power converter. A diagram of the sensor is shown in Fig. 5, and the principal sensor parameters are tabulated in Table III.

To obtain an adequate signal-to-noise ratio from a system whose range resolution is 25 m on the surface and which utilizes a solid-state transmitting device, it is necessary to use a long transmitted pulse and pulse compression techniques to reduce the peak power requirements. The output of the transmitter assembly is, as a result, a linearly swept frequency-modulated pulse (or chirp) having a 634:1 compression ratio. It is generated in a surface acoustic wave (SAW) device located in the chirp generator subassembly of the transmitter
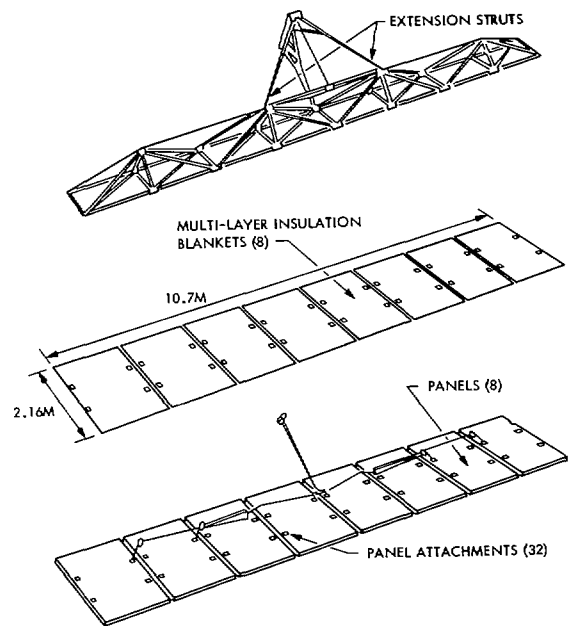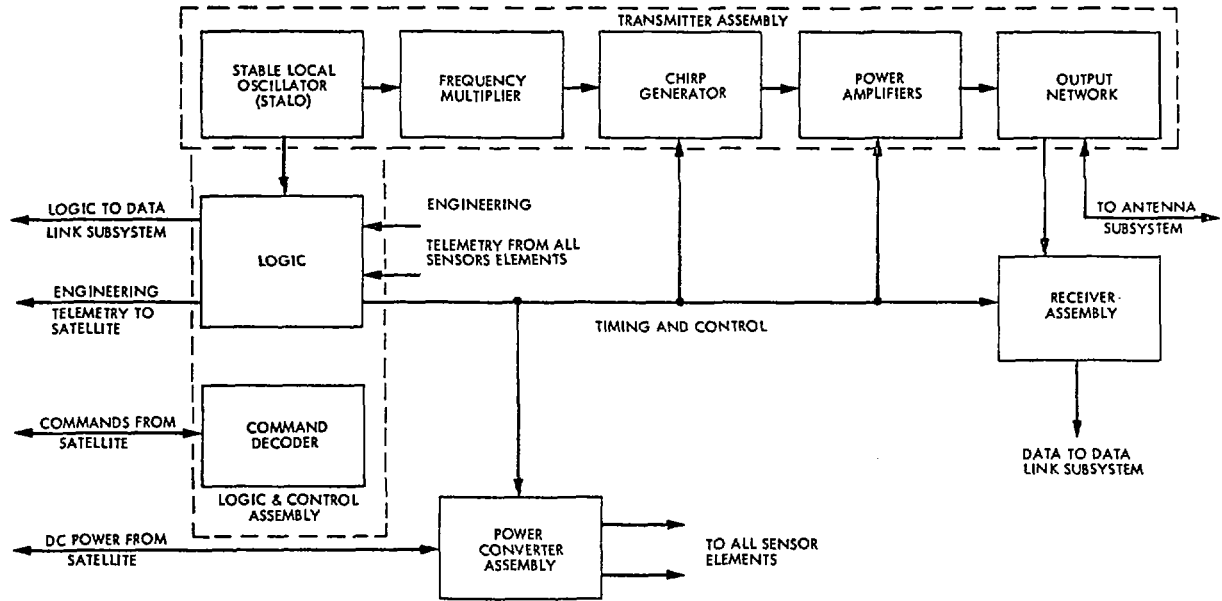
Fig. 5.   Sensor electronics subsystem functional block diagram.

assembly by a 33.8-μs frequency multiplied to (1274.83 MHz) sample of the prime system timing source, the stable local oscillator (STALO). The nominal peak output power level of this pulse is 1000 W.

The output of the three parallel power amplifiers is coupled to the antenna subsystem through an output combiner. A portion of the output (leakage) is also impressed on the receiver input where a load is placed in the circuit each time the transmitter operates. This prevents the leakage pulse from burning out the input stage of the receiver.

Echo returns are coupled into the receiver assembly through the output network in the transmitter. Because the waveform from the nominal sea surface with a uniformly illuminated antenna is expected to vary in intensity in proportion to the variation of antenna gain with angle, a sensitivity time control (STC) has been incorporated in the receiver. The STC action, initiated by satellite stored commands which, in turn, are based upon predictable variations in range from the satellite to the earth's surface along the antenna main lobe centroid, linearly decreases the receiver gain by 9 dB during the first half of the returned echo period, and then increases the gain until the end of the echo has been received. The application of the STC should result in a nearly uniform signal (echo) return, considering a uniform scattering field, and, as a result, the dynamic range required to transmit the resultant data to Earth is reduced by 9 dB.

During the Seasat-A mission, all of radar images gathered during the early passes showed a strong decay in image brightness from the start of the swath to the end of the swath. This was due to an incorrect positioning of the STC window with respect to the swath. This problem was corrected by implementing a software correction to the sensor configuration commands which correctly positioned the STC window with respect to the imaged swath.

The sensor receiver output is sent to the data link along with timing and frequencies derived from the SAR system local oscillator (STALO).

The STALO generates a very stable (in frequency) signal at a nominal frequency f_s, a portion of which is delivered to the multiplier assembly. Another portion of this signal is used to derive both square wave clock and sine wave signals at $f_s/3$, which are used in synchronizing other sensor electronics subsystem functions. The frequency multiplier assembly provides signals of $3f_s$, $9f_s$, and $18f_s$. The $3f_s$ and $18f_s$ signals are delivered to the chirp generator where, along with a portion of the STALO signal f_s, they are used to generate a linear FM pulse (chirp) signal at a frequency of $14f_s$. The signal at $9f_s$ (STALO multiple) and a portion of the STALO signal at f_s are delivered directly to the data-link subsystem along with a signal derived from the PRF event and stalo which divides the interpulse interval into 4096 sectors (COHOD).

The remaining two assemblies in the sensor electronics subsystem are the logic and control and the power converter. They provide the primary electrical interface with the satellite. The logic and control assembly receives commands from the satellite, decodes them, and causes the sensor electronics subsystem to assume one of a number of operating modes. In addition, the logic and control interfaces between the satellite and the intrasubsystem engineering telemetry. The power converter assembly provides the stable isolated power required by the subsystems.

C. Data-Link Subsystem

The purpose of the data-link subsystem is to transmit the radar echo to the ground for digitization, storage, and subsequent processing. The link must also maintain the phase and time references necessary to the processing function, thus providing a unity transfer function. The chosen implementation technique was a linear S-band modulator/transmitter/ receiver/demodulator combination. This choice was governed chiefly by the available frequency spectrum/bandwidth. Furthermore, it appeared that a linear S-band link would
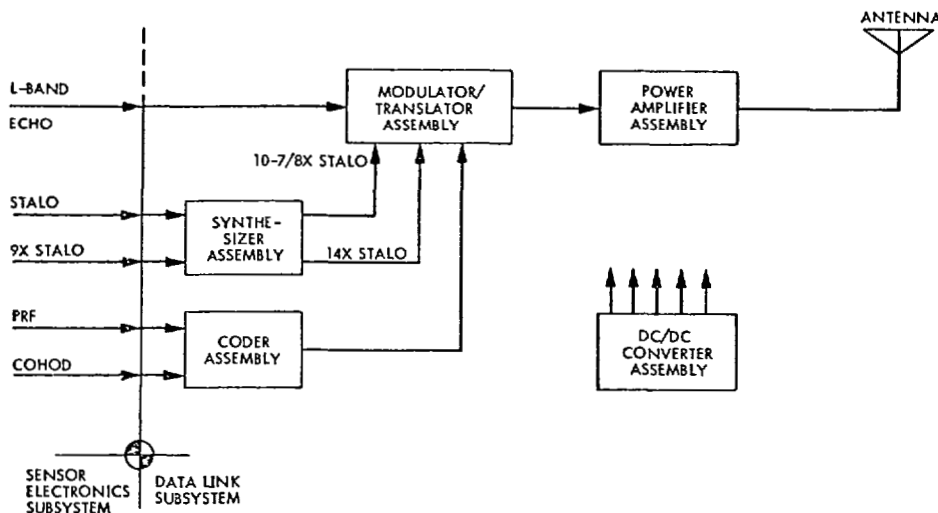
Fig. 6. Data-link subsystem (satellite) functional block diagram.

require minimum advances of the state of the art to return the large data rate generated by the SAR system. The data link was designed and implemented by the Applied Physics Laboratory of Johns Hopkins University.

In addition to the basic requirement for linearity derived from the need to preserve information, the inclusion of necessary phase and timing signals placed an additional burden on the linear property of the link. The data-link subsystem must perform the following functions. On the satellite, the data link must do the following:

a) translate the L-band echo return to S band,

b) orthogonally combine the offset video with both PRF and stable reference,

c) amplify the result linearly (with negligible phase error) for transmission.

On the ground, the data-link subsystem must do the following:

a) translate the composite S-band signal to an offset video frequency centered at 11.25 MHz,

b) coherently demodulate the signal with the spacecraft local oscillator,

c) remove the link-induced Doppler from the composite signal,

d) reconstruct the PRF and STALO signals from the video.

Fig. 6 shows the satellite portion of the data-link subsystem and its interface to the sensor electronics subsystem. The STALO is the master timing and phase reference for the entire SAR system. The 9X STALO is included as a means of mechanizing the synthesizer assembly whose function is to generate the L-band radar frequency and to obtain the frequency translation required to reach the 2265-MHz nominal link frequency. In particular, the L-band frequency is 14 times, the S-band frequency is 24-7/8 times, and the translation frequency is 10-7/8 times the STALO frequency.

The *coder assembly* produces a 4096-bit length pseudorandom (PN) code whose time duration is one interpulse period (IPP). It does so by generating a clock frequency at 32 times COHOD, which itself is 128 times PRF. A twelve-stage shift register and a pulse adding gate produce the 4096-

bit code. Within limits, this function is transparent to PRF changes; and, as a result, the data-link subsystem is slaved to the sensor electronics subsystem.

The modulator/translator assembly performs three functions: modulation of 0° phase component of the 14 times STALO and combination of the result with an equal power 90° phase tone-component; linear addition of the combined reference components to the radar echo at a level 20 dB below the nominal echo power; and translation of the composite signals to S band by mixing with the 10-7/8 times STALO component.

The *linear power amplifier assembly* delivers an output to the antenna assembly of 5 W for a nominal radar echo.

The spectrum resulting from adding the SAR return to the PN encoded PRF event and the pilot carrier is shown in Fig. 7. The function of the ground portion of the data link is to separate these three signals from the composite spectrum and perform the necessary synchronous demodulation in order to recover the target phase.

The ground-based portion of the data-link subsystem operates with standard telemetry ground station front-end components. Fig. 8 shows these elements from the S-band antenna through the S-band parametric amplifier to the down converter, multicoupler, and multifunction receiver (MFR) through to the data-link subsystem demodulator assembly. The MFR tracks the link Doppler-shifted pilot tone, thereby presenting the composite signal to the demodulator assembly at the standard 110-MHz output.

The demodulator assembly detects and tracks the PN code with a noncoherent input/output channel detection at the 110-MHz frequency. A 132.4-MHz VCO frequency is used with multiples of the reference frequency to translate the radar echo to the offset video signal which ranges between 1.88 MHz to 20.88 MHz. The VCO frequency is also used to reconstruct the STALO so that STALO/2 may be delivered to the ADC subassembly in the SAR data formatter (SDF) assembly. All the frequency and phase components of the radar echo are maintained in specific relationship to the STALO frequency.

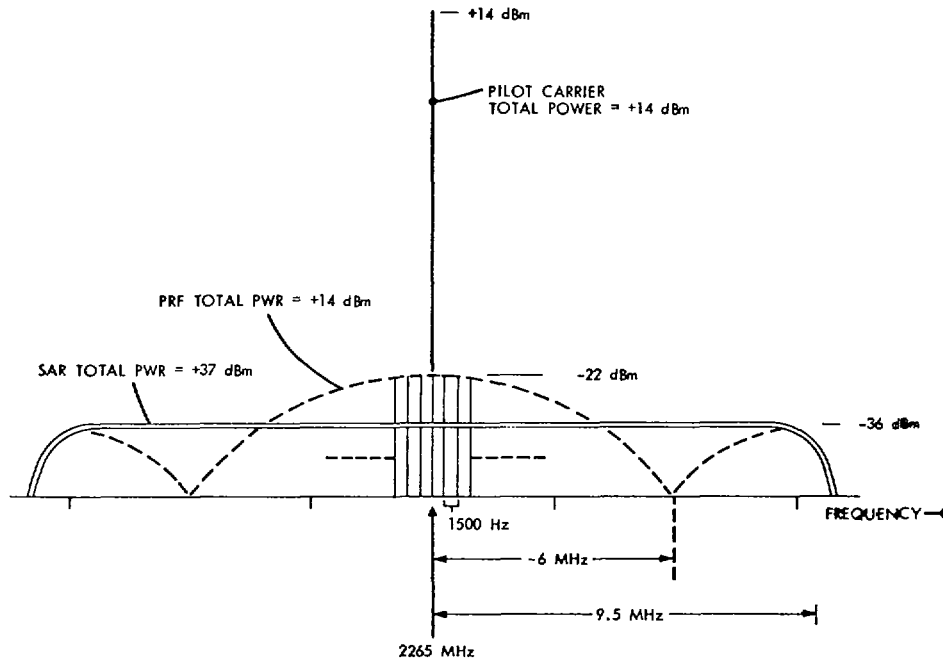The reconstructed PN code is used to develop a coherent

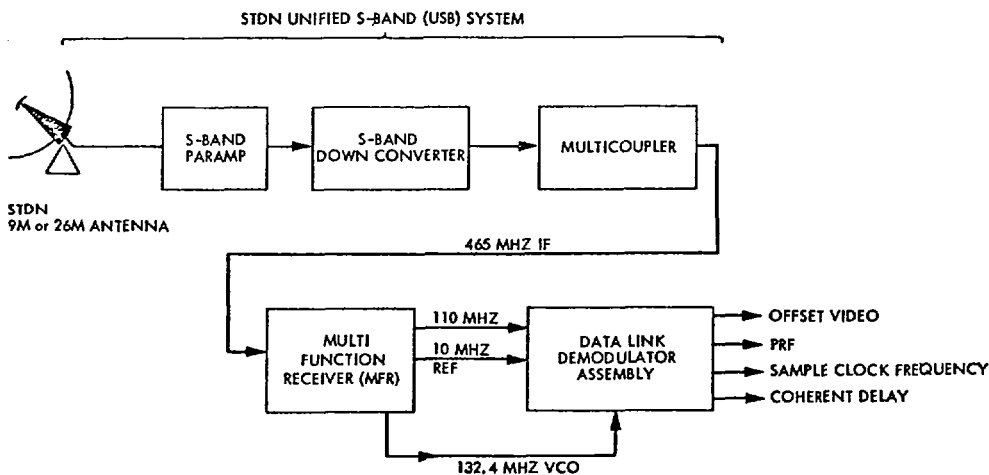Fig. 7. Composite SAR data-link S-band transmitted spectrum.

Fig. 8. Data-link ground assemblies functional block diagram.

delay pulse corresponding to the echo position in time in the interpulse period (IPP).

D. SAR-Unique STDN Subsystem

The SAR-unique space tracking and data network (STDN) subsystem equipment is depicted in the functional block diagram, Fig. 9. The subsystem is composed of three assemblies, the SDF, the high density digital recorder (HDDR), and the SAR simulator (SIM). This subsystem was also designed and built by the Johns Hopkins Applied Physics Laboratory.

The SDF is a specialized device designed to meet particular SAR system requirements. Upon receipt of a trigger signal from the data-link subsystem demodulator assembly, the SDF accepts and digitizes the analog offset video signal furnished by the demodulator. Digitization occurs only during the period (~300 μs) when the SAR video return is expected.

The resulting 13 680 samples, which are generated at a rate of up to 227 Mbits/s, are temporarily stored within the SDF. Information on the operational status of the SDF and the demodulator is also collected and retained. The video samples, the status information, and GMT time are formatted and sent to the HDDR at a rate of about 117.5 Mbits/s. The HDDR records this high rate stream on 1-in wide magnetic tape. Recording uses 40 (of 42) parallel tracks on the tape at a recording speed of up to 150 IPS. Parity is included on each track and timing information is carried on one of the remaining tracks.

The SDF also performs a command timing function. Remotely generated equipment commands which control some SDF and demodulator operations are accepted before each pass by the SDF. Each command includes a time tag specifying when the command is to be implemented. The SDF compares the command time(s) to GMT and issues the
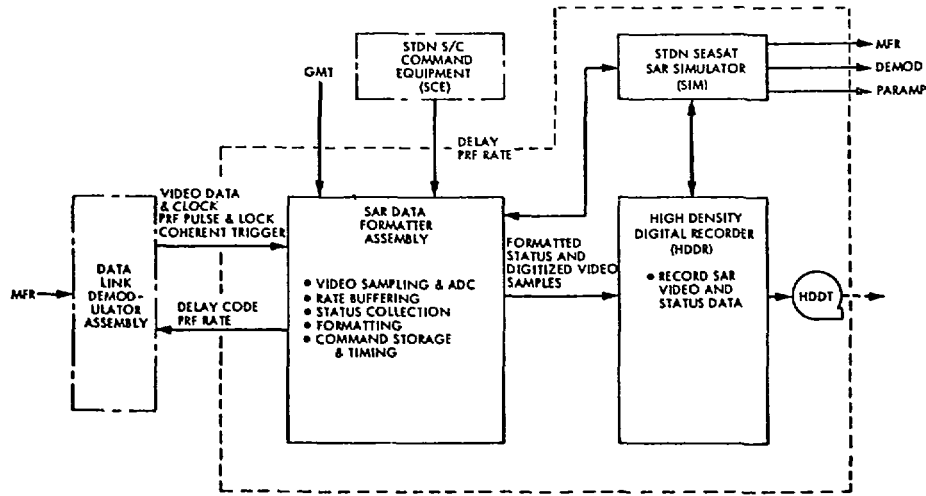
Fig. 9.   SAR-unique STDN subsystem functional block diagram.
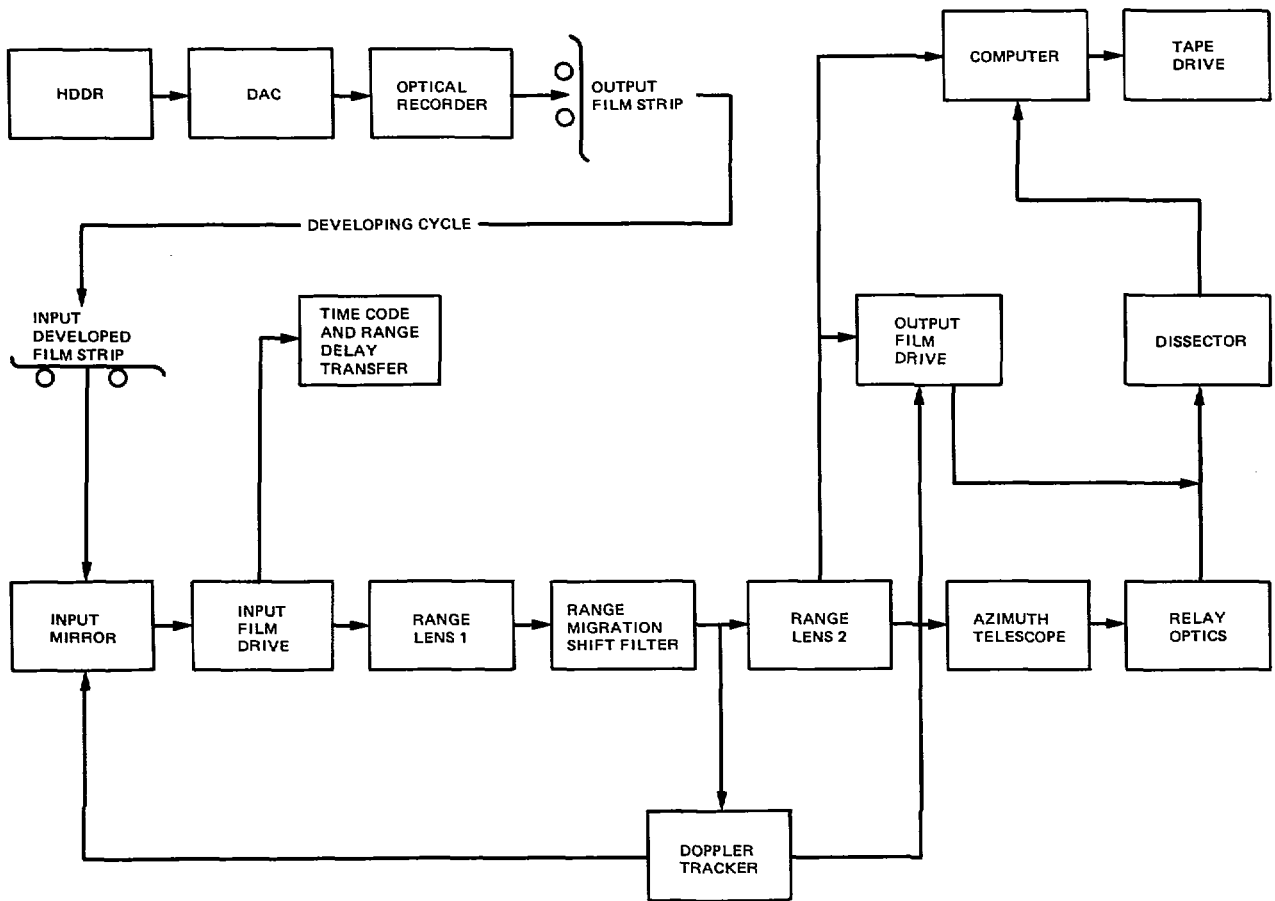
Fig. 10.   SAR data processing subsystem functional block diagram.

command (to itself and the demodulator) at the appropriate time. This timing and command function eliminates time critical manual operations at the station.

E. SAR Data Processing Subsystem

The SAR data processing subsystem (SDPS) provides nonreal-time reduction of the data acquired and recorded each pass. The approximate amount of data per 10-min pass is 10^{11} bits which, using 5-bit quantization, results in 2×10^{10} pixels of raw data per pass. The functional block diagram of the SDPS is shown in Fig. 10.

Digitally recorded data (HDDT) is played back to a film recorder. Time code and range delay (to digitization window) are optically coded in two separate data channels on one side of the SAR echo data. The film drive speed is slaved to predicted spacecraft relative ground speed at swath center.

Four tape passes are made to record the four 1/4-swath strips, having approximately 25 km of width. Before correlation, azimuth Doppler ambiguity must be determined from targets in the data or from attitude information. The Doppler tracking system steers the illumination beam via the input mirror so that the Doppler phase histories are centered in the optical system (the signal for steering ambiguity spectrum with lowest spatial frequencies always given preference to minimize film MTF fall-off effects.

The range migration correction optics are moved in azimuth in synchronism with the input mirror so that the proper correction is maintained.

The azimuth telescope is automatically adjusted to account for range shifts in the digitization window. Demagnification is adjusted for each quarter swath so that unity aspect ratio is achieved at each swath center, then relay optics include a magnification lens to adjust the image scale factor to 500 000:1. The output film drive is tilted above the optical axis in synchronism with the input mirror movements to correct for azimuth data skew caused by Doppler beam steering; also the time code is detected off the signal film and transferred to the image film. Time code and film speed are adjusted to account for Doppler steering.

III. RADAR PERFORMANCE

The input to an SAR system is the two-dimensional radar backscattering surface illuminated by the antenna. The output of the SAR system is a pictorial representation of this radar backscattering surface and the ideal SAR system can be represented by a linear transfer function which introduces no distortions or artifacts.

In the pictorial representation of the radar backscatter distribution, the performance of the imaging radar system can be classified by three classes of performance indicators: 1) the resolving capability of the system, 2) the range of values of detectable radar backscatter coefficients for distributed targets, and 3) the contrast ratio associated with imaging a strong region surrounding a perfectly black region.

To meet the 25-m resolution requirement, a synthetic aperture technique is used, whereby the radar system uses the amplitude and phase of successive returns to synthetically generate a fine resolution antenna. The radar returns from consecutive pulses, as the radar moves along a linear trajectory, are stored and subsequently processed to synthesize an antenna aperture of length equal to the length of the beam illumination on the surface. The resultant along-track resolution is one-half the antenna physical length. Fine resolution across-track is obtained by using a short pulse technique and effectively time-gating the returns. In order to realize a practical system for use in a satellite, a pulse compression technique is used to minimize the peak transmitted power required to get an adequate signal-to-noise ratio. The Seasat system incorporates a 634 to 1 compression ratio.

The ability of the radar system to give an adequate representation of the radar backscatter will be limited on the lower end by the sensitivity of the radar system and on the upper end by the dynamic range of the components com-
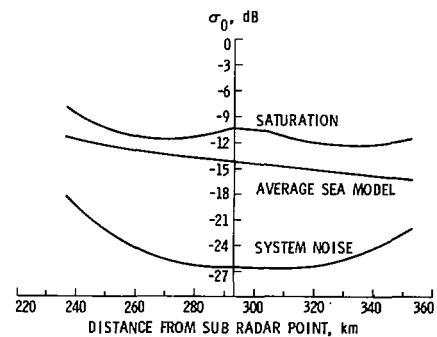

Fig. 11.   Seasat-A SAR system nominal range of detectable σ_0.

prising the radar system. Furthermore, the sensitivity of the radar system will depend on the location of the area beam map with respect to the assigned swath width of the radar system. The predominant element which determines the radar sensitivity as a function of the swath is the radar antenna. The Seasat antenna has a gain which has a peak value of boresight, and as the angle changes from boresight, the antenna gain drops with angle, and consequently, the ability of the radar system to image the earth's surface varies with angular position.

As mentioned above, the Seasat SAR system incorporates a sensitivity time control as an attempt to maintain a constant sensitivity to a radar backscatter. This is possible because the returns from different angles arrive at different intervals of time. The price paid for this time-dependent radar sensitivity is that the radar noise varies across the swath, and consequently, the dynamic range that the overall radar system will have will again change with angular position or swath that is being imaged. If the radar returns are too strong because the radar backscatter is high, then the radar system will exhibit saturation, and consequently, the dynamic range or the ability of the radar system to image over varying values of radar backscatter will be limited.

In the Seasat-A SAR system, the predominant element which exhibits saturation is the analog data link. On the lower end of the radar sensitivity for regions that correspond to the beginning and end of the radar swath, the radar system or radar receiver noise is predominant. At the center of the swath where the sensitivity time control has a minimum gain, the data-link equivalent noise predominates.

In order to accommodate radar signals that are beyond the instantaneous dynamic range of the radar system, the radar receiver incorporates a gain control system to accommodate varying values of radar backscatter. Since the radar system noise, as seen by the data link, is dependent on the gain state of the radar receiver, the overall system sensitivity to measure radar backscatter becomes dependent on the receiver gain state.

For the nominal gain of 89 dB, the performance of the Seasat-A SAR system is as shown in Fig. 11. The upper curve represents the values of radar backscatter which would drive the overall radar system to saturation. As seen from this figure, this curve varies with position that is being imaged. As seen from the curve, for the beginning and end of the radar swath, the values of radar backscatter which will drive the
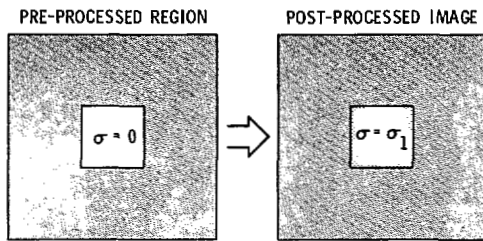
PRE-PROCESSED REGION   POST-PROCESSED IMAGE

$\sigma = 0$ $\sigma = \sigma_1$

Fig. 12.   Contrast ratio of radar imagery.

TABLE IV
SAR SYSTEM ERROR BUDGET

SUBSYSTEM	AMPLITUDE ERRORS	PHASE ERRORS (deg)
Antenna	0.08	5
Sensor	0.04	6
Data Link	0.06	5
Recording/ Processor	0.08	3
TOTAL	0.13	9.7

system to saturation represent targets where radar backscatter is very high. The lower curve represents the threshold for the minimum values of radar backscatter which would appear to have a level that is representative of the overall system noise. Again, the same curve has a higher value at the beginning and end of the area being imaged.

The third class of performance indicators concern the dynamic response of the system to sudden changes in surface reflectivity. Since the radar system can be characterized as predominantly a linear system, the system impulse response will be degraded by amplitude and phase errors in each subsystem and also by system nonlinearities. If the radar system is imaging a region which has no reflectivity (i.e., a perfect absorber) surrounded by a uniformly strong region of radar reflectivity equal to σ_0 as shown in Fig. 12, then after data processing, the image of this area will show that the equivalent reflectivity of the region with the absorber will have a reflectivity of σ_1 which is lower than σ_0. The reason for this apparent reflectivity is that some of the noise passes through the system filter and some of the energy surrounding, the absorber spills into the region of the absorber. How much energy is spilled over from the surrounding region depends on the quality of the subsystem through which the radar signals pass. The quality of these subsystems can be expressed either in terms of the integrated sidelobe ratio or amplitude and phase errors of the subsystem. The various subsystems for the Seasat-A SAR were specified for amplitude and phase errors because the subsystems could subsequently be tested against these factors with standard test equipment. The amplitude and phase error budget for the SAR system components is summarized in Table IV.

The output of the Seasat-A SAR consists of an image on photographic film. The radar data, which is a representation of the radar backscatter map of the imaged surface, has gone through an extensive path, some of which it is not possible to control well enough. The radar data was telemetered to the ground, passed through station receivers, digitized, re-

15 dB

-4   -3   -2   -1   0   1   2   3   4
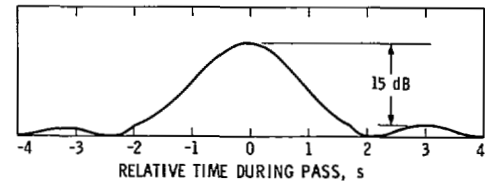RELATIVE TIME DURING PASS, s

Fig. 13.   Recorded azimuth pattern for the SAR antenna.

corded, played back, converted back to analog form, used to intensity modulate a cathode ray tube, imaged on photographic film; the film was developed, radiated with laser light, energy diffracted, and a second film was exposed and developed. However, special care to retain linearity until the last film was taken because any nonlinearities tend to cause image degradation. In view of the complexity required to retain system calibration, the procedure used is as follows. The system gain through the input of the optical recorder was obtained by measuring the receive-only noise power from the system, the pre-flight calibration data of the antenna, and the spacecraft altitude data. In at least one SAR pass, the system receive-only noise was varied by stepping through the various receiver gain states with the transmitter off. The SAR antenna calibration data was verified using portable receivers deployed during selected passes. The SAR antenna pattern in azimuth was obtained by recording the received signal intensity on a strip chart recorder as the satellite passed by the receiver site. Fig. 13 shows the recorded azimuth pattern for one particular revolution. A series of recordings were taken on several satellite passes across the 100-km range swath provided a means of mapping the antenna elevation (range) patterns at several elevation points by recording the maximum signal level detected at each location.

The gain of the optical system from the input of the optical recorder to output image was obtained by injecting calibrated noise at various levels into the input of the optical recorder and measuring the effect at the output image. To assess the performance of the SAR system, the following image quality parameters were measured: 1) resolution, 2) the range of detectable radar backscatter σ_0, and 3) the contrast ratio. Each of these parameter measurements utilized microdensitometer scans of the output image film and the conversion of the film density to relative backscatter power.

Resolution of the SAR system, specified to be less than 25 m, is defined as 0.443 of the null-to-null width of the system impulse response function. Resolution in the azimuth (along-track) direction is dependent upon the number of independent looks for each pixel, and the range resolution (across-track) is dependent upon the local incident angle, and thereby, the relative location in range in the image swath. An array of corner reflectors of various sizes, each spaced 300 m apart, was deployed in the Goldstone Dry Lake area of California. Fig. 14 shows the imaged corner reflector area.

These reflectors served as point targets, the impulse response of which were imaged and measured for null-to-null widths both in the range and azimuth directions. The measurements indicated that the range resolution was less than 25 m and the azimuth resolution was approximately 40 m. The ap-
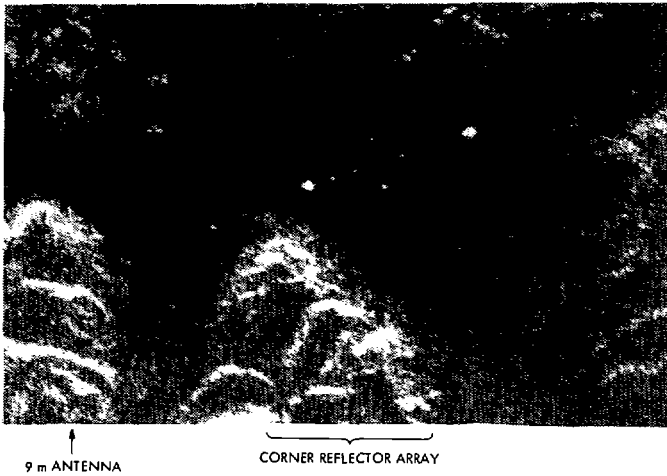
Fig. 14. SAR imagery of corner reflector array at Goldstone.
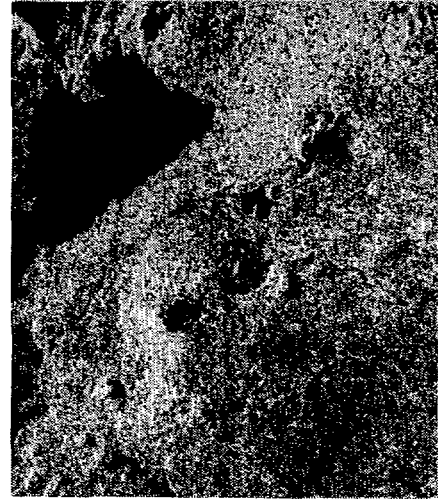
9 m ANTENNA   CORNER REFLECTOR ARRAY

Fig. 16. SAR imagery of the Charlton Lake area.

Fig. 15. SAR imagery of the Saline Valley.

Fig. 17. SAR imagery of the Southern California coastline.

parently excessive width in the azimuth direction is most likely due to irregularities in the film drive mechanism for the signal film and image film.

Detectable (or dynamic range) σ_0 from an uniform surface ranges from a minimum which is equal to the system noise (noise equivalent σ_0) to that σ_0 which saturates the SAR system. The system was specified to detect σ_0 from -25 dB to 5 dB, corresponding to a dynamic range of 30 dB with receiver gain changes. Because of effects which include the antenna gain shape and the sensitivity time control compensation in range, the range of detectable σ_0 varies across the swath. Also, the receiver noise level, and therefore, the receiver gain, affect the noise equivalent σ_0. Image film density was measured across the swath for distributed targets and the dynamic range varied from 13.2 dB in the near range to 9.6 dB in the far range for one particular Seasat-A pass. Measurements using other passes in which the Saline Valley, California, was imaged indicated dynamic ranges as high as 16 dB, limited by the dynamic range of the output film. Fig. 15 shows the SAR image of the Saline Valley area. All of these measurements were made for the nominal SAR receiver gain of 89

dB. With the use of actual sea state information from ships off the Baja Peninsula, SAR imagery indicated a noise equivalent σ_0 of -21 ± 5 dB.

The ability of the SAR system for obtaining values of radar backscatter were demonstrated by analyzing several areas in the Death Valley region. These images were imaged and absolute values of radar cross section computed. The results of these measurements, as compared with aircraft measurements indicates ability to measure absolute radar cross section within 2 to 6 dB for the Seasat-A SAR system.

Image contrast ratio is the ratio of energy contained in the main lobe portion of the system impulse response to the energy contained in the area outside of the main lobe, and is specified to be less than 9 dB. This parameter includes the effects of system noise, the ambiguous returns, and the integrated sidelobe energy thus causing contrast ratio to be highly scene dependent. It is possible to bound the contrast ratio by examining the system response to a sharp transition in reflectivity. The water to land boundary of the Charlton Lake, Oregon, was selected for the measurements; Fig. 16 shows the Charlton Lake area. The upper bound of the contrast ratio for these particular measurements was 7.5 dB with average values in the region of 10 to 13 dB.

The basic performance of the Seasat-A SAR system can be summarized that all of the performance parameters have been met on at least some of the imagery. Some of the data were digitally processed and their results confirm this conclusion. Perhaps the crux of the Seasat-A SAR radar perform-

ance can be seen in the quality of final imagery as shown in Fig. 17 showing the Southern California coastline. Certainly, the concept of spaceborne radar sensing is viable and has been proved with the Seasat-A SAR.

ACKNOWLEDGMENT

The Seasat-A SAR system is the result of the dedication of many individuals whose contributions were essential to the design, fabrication, and operation of the hardware itself. These include NASA personnel, the staffs of the Jet Propulsion Laboratory, the U.S. Geological Service, Lockheed Aircraft, the Applied Physics Laboratory of Johns Hopkins University, Ball Brothers Aerospace, M. Marietta, Westinghouse, Goodyear Aerospace, and others. Without their dedication, this experiment would not have been possible.

REFERENCES

[1] L. J. Porcello et al., "The Apollo lunar sounder system," Proc. IEEE, vol. 62, pp. 769–783, June 1974.
[2] J. S. Zelenka, W. D. Hall, and N. G. Massey, "Optical processors and displays for synthetic aperture radar systems," in Proc. Electro Optical Systems Design Conf., New York, Sept. 1972.
[3] W. M. Brown and L. J. Porcello, "An introduction to synthetic aperture radar," IEEE Spectrum, vol. 6, pp. 52–62, Sept. 1969.
[4] R. L. Jordan and B. L. Huneycutt, "SEASAT-A synthetic aperture radar performance," Int. Conf. Communications, Boston, MA ICC'79, June 10–13, 1979.

Visible and Infrared Radiometer on Seasat-1

P. McCLAIN, R. MARKS, G. CUNNINGHAM, AND A. McCULLOCH

Abstract—The visible and infrared radiometer (VIRR) is a scanner for the collection of digital data in the visible and thermal-infrared portions of the spectrum over broad swaths of the earth's surface [1]. Some of the essential electronic and mechanical details of the system are described; and the results of an engineering assessment of its operation in orbit are given. The set of algorithms used to transform the raw VIRR data to calibrated geophysical measurements is discussed. Some of the results of a preliminary geophysical evaluation are presented.

I. INTRODUCTION

THE VISUAL and infrared radiometer (VIRR) on Seasat was a supporting instrument system whose principal function was to provide images of visual reflection and thermal-infrared emission from oceanic, coastal, and atmospheric features that could aid in interpreting the data from the other Seasat sensors. The VIRR was also expected to provide some derived quantitative measurements such as sea surface temperature and cloud top height.

Except the VIRR, all the instruments onboard Seasat were microwave sensors, either active or passive, of which only two were imaging systems. The VIRR enabled the generation of images encompassing the data swaths of all other Seasat sensors, and the ground resolution of the VIRR data was equal to or greater than that of any except the synthetic aperture radar (SAR) and the altimeter. Thus investigators can generally determine whether the field of view of their instrument was partly or completely filled by cloud cover; something about the cloud type and height; confirm the presence or absence of land; possibly detect ocean thermal fronts; and determine the presence of hurricanes, severe storms, and other meteorological features.

II. DESCRIPTION OF THE VIRR

The VIRR was an unused scanning radiometer (SR) originally built for the improved Television and Infrared Observation Satellite (TIROS) operational satellite (ITOS) series [2] of the National Oceanic and Atmospheric Administration (NOAA). Principally because of data rate limitations, the images generated form the VIRR were degraded twofold in the thermal infrared (IR) and fourfold in the visual range (VIS) with respect to the full capability of the original ITOS design.

The VIRR was a two-channel scanning radiometer with one channel operating in the visible region of the spectrum, the other in a spectral region of strong atmospheric transmission in the infrared (see Table I). Scanning was accomplished by means of a rotating mirror mounted at 45° to the optical axis of the collecting telescope. The mirror rotates continuously, creating a line scan perpendicular to the orbital motion of the spacecraft. The motion of the spacecraft provided the second dimension of scan. The scan rate is normally adjusted such that the satellite ground motion at nadir is equal to one resolution element, thus creating a raster with each scan line adjacent to the previous one. In the case of the VIRR, the radiometer was originally designed to operate at 1600-km altitude rather than the 800 km of Seasat; con-